AUTONOMOUS DETECTION OF TRANSIENT PHENOMENA ON PLANETARY BODIES. M. K. Bunte[1], Y. Lin[1], S. Saripalli[1], and R. Greeley[1], [1]School of Earth and Space Exploration, Arizona State University, P.O. Box 871404, Tempe, AZ 85287 (Melissa.Bunte@asu.edu).

Introduction: We assessed the effectiveness of employing autonomous supervised classification techniques to detect transient geophysical phenomena such as volcanic plumes and comet outgassing in spacecraft images. Our objective was to autonomously detect manually verified features in images under onboard conditions. Success enables these methods to be applied to future missions and facilitates immediate detection of transient events and features regardless of viewing and illumination effects, electronic interference, and physical image artifacts. Using images from the Voyager, Galileo, New Horizons, Cassini, and Deep Impact EPOXI missions, we demonstrated successful detection of known plumes on the planetary satellites Io and Enceladus and outgassing on the comet 103/P Hartley 2. We found a positive detection rate of 93% for Cassini images of Enceladus, 74% for New Horizons images of Io, 73% for Galileo images of Io, 95% for Voyager images of Io, and 94% for EPOXI images of Comet Hartley 2. Additionally, we showed that similar techniques are applicable to differentiating geologic features which exhibit similar appearances.

Background: Spacecraft missions have identified active transient events on multiple planetary bodies: explosive and effusive eruptions on Io, geyserlike ejections on Enceladus and Triton, and outgassing of comet nuclei. These phenomena provide key constraints for subsurface processes, interior dynamics, surface-interior interactions, and models of planetary composition [1-4]. Characterizing these events requires sustained observations that are memory and bandwidth depletive [i.e., 5]. The ability to process observations onboard could facilitate monitoring campaigns and optimize science value of returned data by preserving memory and bandwidth for high priority observations.

Recent developments in onboard algorithms allow detection of dust devils on Mars by background subtraction [6], expose Europa's salient features in hyperspectral images [7] using a superpixel endmember algorithm [8] and reveal volcanic plumes on Io [9, 10] and outgassing on comets [4] where features are bright and extend beyond the limb. We combine feature extraction with supervised classification techniques to overcome limitations of these methods, which require a single strong edge, limb-views, sequential observations, or similar views from multiple instruments.

Method: We examined uncalibrated images to simulate onboard data conditions. We applied a Scale Invariant Feature Transform (SIFT) [11] to produce interest points and feature descriptors based on gradient orientations near each point (Figure 1, *left*). Descriptors are invariant to illumination or viewpoint changes, noise, rotation, and scaling. Descriptors for a random selection of images from each dataset were manually categorized by the presence of plumes. Descriptor for the remaining images were tested using the positive or negative designation. We utilized several classification techniques and found that K-Nearest Neighbor (KNN) [12] was most efficient for classifying SIFT features.

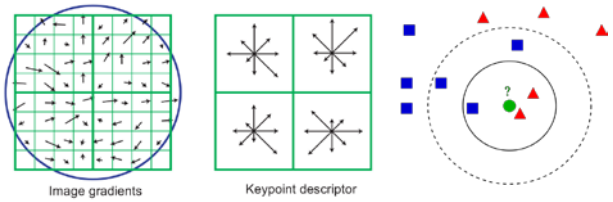

Fig. 1. Keypoint descriptors [*from* 11]: (*Left)* The gradient magnitude and orientation at each sample point near the keypoint are (*Middle)* binned by subregion (here, a 4x4 grid) to generate orientation histograms. Arrow length corresponds to the sum of the gradient magnitudes near that direction within the region. KNN Classification [*from* 13]: *Right*: Classify the sample (dot) according to the most common class within the threshold distance, *k*. Here, the inner circle is *k*=3; the sample is classified as a triangle.

K Nearest Neighbor: In KNN, a feature vector is classified based on the majority class within a neighborhood defined by Euclidean distance (Figure 1, *right)*. KNN does not require a particular spatial distribution of feature vectors and is thus adaptive to unpredictable plume characteristics. Given the high ratio of negative to positive features, a plume will be surrounded mainly by negative features; therefore the smallest *k* is most appropriate to classify a feature; we found $k = 1$ to best discriminate classes. Figure 2 shows the keypoints and features detected with SIFT + KNN.

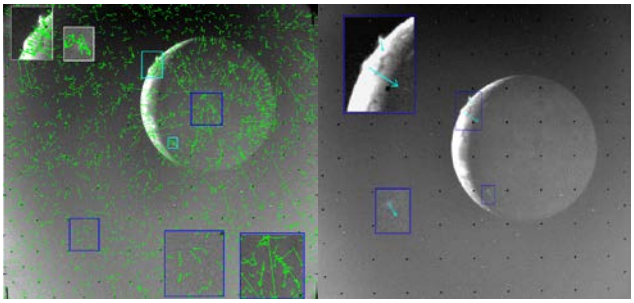

Figure 2. SIFT + KNN. *Left*: Voyager image of Io with SIFT keypoints (green arrows); Light blue boxes outline known plumes (insets, upper left); dark blue boxes correspond to sample SIFT features (insets, lower right). *Right*: Features detected by SIFT + KNN (blue arrows): 2 plumes on the limb; 1 at terminator in shadow (insets).

Results: We applied SIFT+KNN to all images of Io and Enceladus from four missions (Table 1) and observed that detection rates for the Voyager and Cassini datasets were significantly higher than for the other datasets (Figure 3); we attribute this to a smaller variety of plume characteristics in these images. In EPOXI images of Comet Hartley 2, we found that more individual jets were detected than with previous methods [10]. SIFT+KNN detected plumes of different shapes, sizes, and orientations. The most notable improvement over previous methods is the ability to detect plumes that do not extend beyond the planetary limb (Figure 2). Detections were successful in noisy images and when bright artifacts or features were present but failed where plumes were lost in glare or classification failed.

Mission		1st trial	2nd trial
	Test Images	Detection Rate	Detection Rate
Cassini	23	93.30%	88.20%
New Horizons	44	70.00%	74.29%
Galileo	11	67.67%	72.73%
Voyager	81	95.14%	92.47%
EPOXI	23	94.15%	94.37%

Table 1. Statistics of plume detection for each image set

Variations in the classification techniques and multiple random selections of images served to train the classifier to distinguish certain characteristics and to ensure that results were independent of image selection. SIFT features mainly resulted from surface material gradients and background noise, resulting in a high ratio of negative features to positive features in training. The mis-classification rate can be reduced by 1) enlarging the training set at the expense of autonomy as it necessitates further manual interaction, or 2) reiterating the classification process to include training features that have already been classified and re-classified features that were mis-classified in the first iteration at the expense of increased false detections.

In addition to positive plume detections, the methods employed here allow the classification and detection of other features, most notably mountain slopes (Figure 3, *bottom right*). Mountains often appear similar to plumes as bright surface features against the background surface; more favorable viewing conditions reveal their texture and topography. They are tall enough to extend beyond the limb and so would be detected by edge detection methods. Adding a new feature classifier to our training set used with KNN resulted in their accurate detection despite similarities.

Future Work: Future work includes the application of this method to the remainder of all planetary images where plumes are known or suspected to exist and an effort to develop algorithms for the detection of plume deposits which are not extended above the surface but do have characteristics distinct from the background surface. Plume deposits have been observed to change over time as new materials are deposited and old materials are degraded or chemically altered; studying changes in appearance has allowed us to monitor the activity of plumes over the timespan of all spacecraft missions [14].

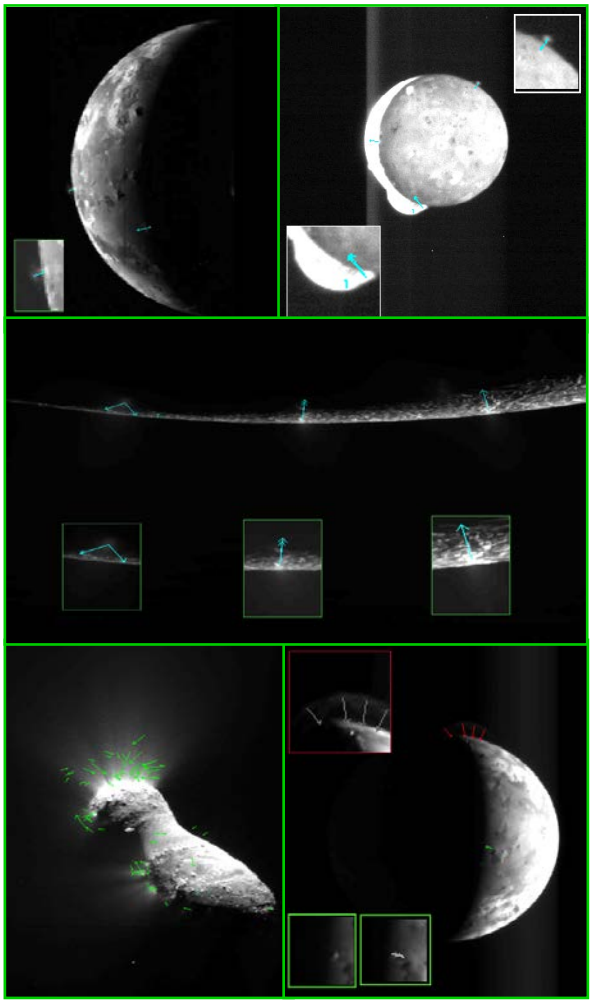

Fig. 3. *Left to Right, from Top*: Plumes detected in Galileo and New Horizons images of Io, Cassini image of Enceladus, and EPOXI image of Comet Hartley2. *Bottom Right:* Mountains are distinguished as separate feature class (red: plumes, green: mountains).

References: [1] Porco, C. et al (2006) *Science 311*, 1393. [2] Lopes-Gautier, R. et al. (1999) *Icarus 140*, 243. [3] Smith, B. et al. (1979) *Science 206*, 927. [4] Hearn, M. A. et al. (2011) *Science 332*, 1396. [5] Clark, K. B. (2007) *IEEE Aerospace Conf. 3-10*, 1. [6] Castano, A. et al. (2008) *Machine Vision & App., 19*, 467. [7] Bunte, M. et al. (2011) *LPS XLII* Abs. #1888. [8] Thompson, D. R. et al. (2010) *Trans. Geosci. & Remote Sens., 48 (11)*, 4023. [9] Bue, B. et al. (2007) *LPS XXXVIII*, Abs. #1717. [10] Thompson, D. R. et al. (2011) *Planet. & Space Sci.* doi.10.1016/j.pss.2011.11.006. [11] Lowe, D. G. (2004) *Int'l Jour. Computer Vision 60, (2)*, 91. [12] Cover, T. M. and Hart, P. E. (1966) *Trans Info. Theory, 13 (1)*, 21. [13] (2007) http://en.wikipedia.org/wiki/K-nearest_neighbor_algorithm. [14] Geissler, P. E. and Goldstein, D. B. (2007), In: *Io After Galileo*, Lopes, R.M.C. and Spencer, J. R. (Eds.), 162-192.